

Wood Physics/Mechanical Properties

Mojtaba Hassan Vand*, Patrik Nop, Valentino Cristini, Jan Zlámal, Vít Šeda and Jan Tippner

An investigation of mechanical properties of linden green wood

https://doi.org/10.1515/hf-2024-0110 Received November 21, 2024; accepted February 19, 2025; published online March 12, 2025

Abstract: This article investigates the mechanical properties of linden green wood, setting out the results of three approaches to assessing tree stability and strength aimed at improving the safety evaluation of living trees. Due to the high moisture content (MC) of green wood and its significant impact on its mechanical properties, data from dried specimens cannot be used to model green wood behaviour. The research was carried out on wood samples with both 40 % and 60 % MC. A non-destructive test (NDT) assessed specimens and measured their vibro-acoustic material properties. Subsequently, destructive static tests were conducted along the three main orthotropic axes of the wood samples. The resulting data led to the development of a bilinear orthotropic model and a comprehensive dataset covering both elastic and plastic material properties. Next, the material properties were optimised to compute and validate a numerical model using the finite element method (FEM). By refining the material properties, the FEM predictions closely matched the experimental results, with a maximum error of 5%. This information on the wood's experimental, FEM and NDT-derived properties offers an excellent basis for evaluating linden green wood for many applications.

Keywords: green wood; linden; non-destructive test; modal analysis; frequency-resonance method; bi-linear elastoplastic modelling

1 Introduction

Most of the mechanical properties of wood are influenced by its moisture content (MC). Green wood, with MC values over the fibre saturation point (FSP) of 30–200 %, has very different mechanical properties from dried lumber (Glass and Zelinka 2021). Extensive knowledge of the mechanical properties of dry wood exist due to its commercial value (Niklas and Spatz 2010), but the properties of green wood are less well known. This knowledge gap is a disadvantage for tree biomechanics when assessing the stability of living trees (Dahle et al. 2017).

Tests were conducted on linden green wood to determine its static and dynamic mechanical properties and used these as inputs in finite element method (FEM) modelling. These property values then optimised to enhance FEM modelling accuracy, validated by comparing FEM results with two sets of experimental data. The offered information is suitable for FEM modeling of dynamically loaded structures such as tree branches and stems, enabling strength assessments under various conditions, such as high winds. However, the presence of knots and other defects, which can significantly influence a tree's mechanical behavior, presents a considerable challenge to accurate modeling and needs further attention.

Tilia is a common tree genus found in the temperate latitudes of the northern hemisphere. There are approximately 40 species in the genus, many of which have been little studied (Korkut 2011). As its wood is soft and prone to rotting, linden has little value as a source of timber, though the trees are ornamental and are commonly planted in city streets and parks. They are successful as urban decoration also because of their resistance to air pollution – including from traffic – and severe pruning (Kunneman and Albers 1991). With so many lindens planted in cities, knowing more about the mechanical properties of their green wood could help prevent incidents of trees falling on roads. Many factors can affect the stability of a tree, such as its age (Stokes 1999), the weather (Lundström et al. 2008) and other regional conditions (Spatz and Pfisterer 2013). Understanding how these affect trees could help city officials predict trunk failure and avoid uprooting (Detter et al. 2019) in high winds

^{*}Corresponding author: Mojtaba Hassan Vand, Faculty of Forestry and Wood Technology, Department of Wood Science and Technology, Mendel University in Brno, Zemědělská 3, 613 00 Brno, Czech Republic, E-mail: xhassanv@mendelu.cz. https://orcid.org/0000-0001-8747-6973

Patrik Nop, Valentino Cristini, Jan Zlámal, Vít Šeda and Jan Tippner, Faculty of Forestry and Wood Technology, Department of Wood Science and Technology, Mendel University in Brno, Zemědělská 3, 613 00 Brno, Czech Republic, E-mail: patrik.nop@mendelu.cz (P. Nop), valentino.cristini@mendelu.cz (V. Cristini), jan.zlamal@mendelu.cz (J. Zlámal), vit.seda@mendelu.cz (V. Šeda), jan.tippner@mendelu.cz (J. Tippner)

(Peltola 2006). The effects of such weather conditions can be simulated in tests that require knowledge of the mechanical properties of green wood, such as classic static pulling tests (Brudi and van Wassenaer 2002) and destructive pulling tests (Kane and Clouston 2008). Impact tests on green wood samples can provide valuable information for assessing tree stability under impact loadings (Hassan Vand and Tippner 2024).

Non-destructive testing (NDT) is a powerful tool for determining mechanical properties, assessing and evaluating the quality of products and detecting defects and damage in materials (Guyott et al. 1986). Its widespread adoption shows its potential for assessing wood (Vössing and Niederleithinger 2018), particularly in situations with considerable limitations such as heritage structures (Hum-Hartley 1978). Various non-destructive methods are available for assessing wood and wood-based materials, including the drilling resistance technique, electromagnetic radiation method, colour gloss spectroscopy, moisture measurements, thermography, electrical resistance tests, acoustic tomography and eigenfrequency measurements (Niemz and Mannes 2012). Resonant frequencies can be determined from impactinduced vibrations by striking a specimen with a small hammer (Hassan et al. 2013). NDT methods developed for small wood beams allow the material properties of the outer wood of standing trees to be determined and are useful in the detailed, localised evaluation of elastic wood properties (Ilic 2003). Šilinskas et al. (2021) used an acoustic velocity measuring system to determine the dynamic modulus of elasticity (MOED) of small-leaved linden tree wood to assess its quality. With improving NDT methods, databases of material properties have been developed for various applications (Borůvka et al. 2020). In the longitudinal direction, shear modulus based on transversal waves can be determined by considering the speed of sound and the density of the material (Ilic 2001).

The mechanical behaviour of wood depends on the species and the moisture content (Schneeweiß and Felber 2013). Other parameters can have an effect, such as the size of the piece of wood, since larger pieces are more likely to have knots and defects than smaller ones (Büyüksarı et al. 2017; Schlotzhauer et al. 2017). A combination of mechanical tests is sometimes used to determine material properties (Kandler et al. 2015), although, standards, methods, and assumptions may produce slight differences (Kovryga et al. 2020). Saliklis et al. (2003) presented a nonlinear constitutive material model for orthotropic materials as a bilinear stressstrain curve. Milch et al. (2016) established an elastoplastic material model based on the Hill's yield criterion, including nonlinearity and isotropic hardening. Babiak et al. (2018)

examined the difference in modulus of elasticity (MOE) readings resulting from three-point and four-point bending tests. Huang et al. (2020a,b) studied the nonlinearity of the deformation of cellular wood structure under compression load in the radial direction. Lundström et al. (2007) explored the bending, density and growth characteristics of green wood such as the MOE and modulus of rupture (MOR). Niklas and Spatz (2010) explored the relationships between the density and other mechanical properties of green wood. Using mechanical tests, FEM and optimisation methods, Zlámal et al. (2024) derived the mechanical properties of beech green wood, which can be used to determine the properties of other species with similar wood structures.

Digital image correlation (DIC) method is a non-contact optical measurement technique widely used to analyse surface deformation and strain. It offers full-field measurements of shape, deformation and motion with high precision and efficiency (Sutton et al. 2009). The versatility of DIC makes it suitable for applications ranging from small wood specimens (Zink et al. 1995) to living trees subjected to bending forces (Sebera et al. 2014) and across material behaviours from elastic deformation to failure (Hild and Roux 2006). The technique is valued for its quick, accurately and cost-effective results. A notable application of DIC in wood-related studies is the determination of multiple material properties of solid wood from only a single test (Brabec et al. 2015, 2017; Pan et al. 2009). However, reaching the method's excellent accuracy requires extra attention how to implement the method (Pan 2011).

FEM can be used to reduce the time required to analyse and predict the mechanical behaviour of materials (Smith et al. 2007). From precise data, engineers can develop detailed models and reliably forecast the mechanical behaviour of products (Cecháková et al. 2012). FEM offers significant advantages over other methods of assessing trees mechanically, including reduced time and cost. For accurate FEM modelling of wood, precise knowledge of its mechanical properties is necessary (Mackerle 2005). Some researchers have proposed using an isotropic hyperelastic model to evaluate the transverse compression and densification of cellular materials through computer modelling software (Aimene and Nairn 2015). However, an appropriate model for wood should account for its orthotropic nature, accommodate plasticity when stresses exceed the yield limit and reliably predict failure (Zlámal et al. 2024). The derived material properties have the same quantity, and the output of these tests can be used indefinitely for further FE analysis (Fajdiga et al. 2019; Hu et al. 2021; Milch et al. 2016). Although the modeling of wood by FEM needs some extra further attention about wood's nature from considering wood as a

defectless material to a material with defects such as presence of knots and the grain deviation (Briggert et al. 2016; De Borst et al. 2013; Guindos and Guaita 2013; Guindos 2014; Hackspiel et al. 2014). The influence of moisture content is considerable during modelling wood in FEM (Autengruber et al. 2020), and this effect can change over time (Fortino et al. 2009).

2 Materials and methods

2.1 Preparation of test samples

The linden (Tilia cordata Mill.) timber was collected from an urban reconstruction site in Brno, Czech Republic, Four trees were selected and cut into lumber for further processing. From fresh wood in each tree, a 2 m long log was taken from the lower part of the stem (above the root flares). From each log, samples were prepared for mechanical testing and visually inspected to avoid knots and defects. Samples were divided into two groups and treated to provide each with a different moisture content. Samples for the higher moisture content (HMC) group were submerged in water for seven days. They were then acclimatized for another seven days airtight sealed chambers with half water and the samples were above the water level. This process aimed to achieve a MC in laboratory temperature in the range of 50–70 %. For the lower moisture content (LMC) group, samples were acclimatized above water level for seven days immediately after cutting. This resulted in laboratory temperature to an MC range of 30-50 %. Figure 1 shows the shape and dimensions of the test samples, and Table 1 lists the number of samples for each test from the HMC and LMC groups.

2.2 Non-destructive testing

All bending specimens were tested using the frequency resonance technique (FRT) before destructive testing. This test consists of striking a rubber mallet at the midpoint of a beam fixed by foam supports at the nodal points of the first bending mode shape; calculations are made of the MOED at longitudinal-tangential (LT) and longitudinal-radial (LR) directions and the damping coefficient ($tan\delta$) of bending vibrations. Oscillations were sensed using a Doppler's laser vibrometer PDV-100 (Polytec GmbH, Germany), and were recorded using the dynamic signal acquisition module DEWE-41-T-DSA of DEWESoft (DEWETRON, Inc., USA). The natural frequencies were determined using the Fast Fourier Transform (FFT) algorithm, processed using MATLAB® v2021 (The MathWorks, Inc., USA) (Hassan and Tippner 2019). MOED was calculated from the first natural frequencies which corresponded to the first bending mode by the following equation:

$$MOED_{t/r} = \left(\frac{2f_{LT}}{2.25\pi}\right)^2 \frac{mL^3}{I_{t/r}}$$
 (1)

where f is the frequency of the mode used (first bending mode in t/r direction), m is the mass of the specimen, L is the length of the specimen, and I is the moment of inertia of the cross-section. $\tan\delta$ was determined from the signal using the logarithmic decrement of damping (LDD) as the amplitude decrease base in Equation (2),

$$\tan \delta = \frac{\text{LDD}}{\pi} \tag{2}$$

where LDD indicates the decrease in damped oscillations amplitude in the range of the maximum amplitude and the amplitude closest to 5 % of the maximum. LDD is calculated from the results of the logarithm of the ratio of successive

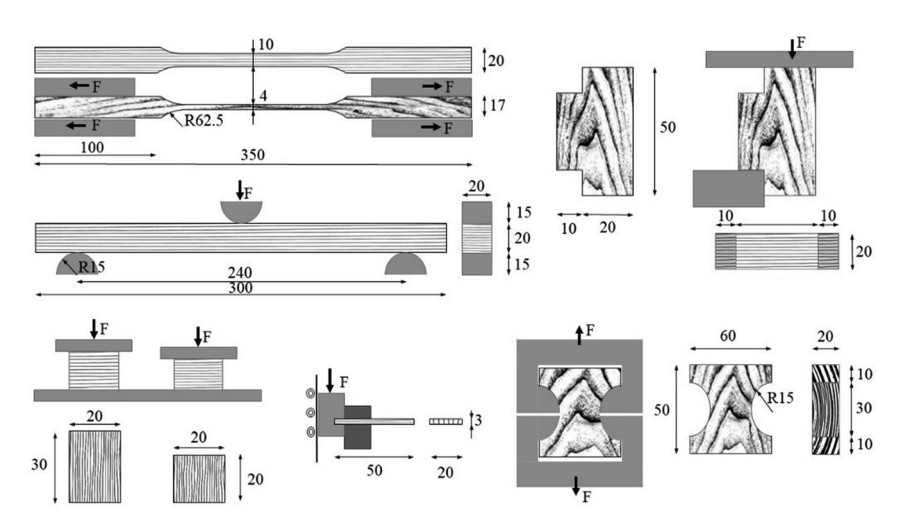


Figure 1: The shapes and dimensions of the test samples (in mm) adapted from Tippner et al. (2022).

	НМС	LMC	Total		НМС	LMC	Total	
Shear LR	20	20	40	Compression LT	20	18	38	
Shear LT	20	20	40	Compression RL	14	8	22	
Shear RT	20	20	40	Compression TL	15	10	25	
Tension L	32	20	52	Compression TR	13	19	32	
Tension RL	19	20	39	Compression RT	9	20	29	
Tension TL	19	18	37	Bending	19	18	37	
				Comp LR	19	20	39	

Table 1: The number of high moisture content (HMC) and low moisture content (LMC) samples for each test.

amplitudes shown in Equation (3), where a_n and a_{n+1} are the amplitudes of successive vibration cycles. To increase the robustness of the results, LDD was taken as the average of the results of 10 hits.

$$LDD = \ln \frac{a_n}{a_{n+1}} \tag{3}$$

The dimensions and mass of the bending and compression samples were measured immediately before the NDT, after the destructive tests and following kiln drying until stable conditions were achieved. Their MC and densities (both green and basic) were determined from their dimensions after conditioning state and the masses of both dried and wet states. The results of the NDT were tested statistically to determine if the effect of MC was significant.

2.3 Static mechanical testing

A universal testing machine (ZWICK Z050, Zwick, Germany) was used in an experimental set up based on Czech standards ČSN 490115 (1979) and ČSN 490116 (1986). The stress was determined by the loading force of the samples as recorded by the control software (TXpert version 11.02, Zwick, Germany) of the universal testing machine. The DIC method was used to calculate the deformation and consequently the strain in each test from the relative movement of different points of the samples. DIC was not used for the tension test parallel to the grain or the RT shear test due to the narrow dimension of the specimens (10×4 mm); instead, a set of extensometers connected to the testing machine was used. Two charged-coupled device (CCD) cameras with a resolution of 2,452 × 2,056 pixels (AVT Stingray Copper F-504, TKH Group N.V., Germany) equipped with Pentax C2514-M lenses (Ricoh Company, Ltd., Japan) recorded the experiments. The surface of all samples was painted in a black speckled pattern, intended to improve the accuracy of the DIC method in determining the deformation and strain pattern of the samples. The captured images were processed

by Video extensometer Mercury RT® software (Sobriety, Czech Republic) which allows multiple virtual displacement probes to be applied and advanced image features to be tracked. The relative displacement of the software probes indicated the strain in each direction alongside and perpendicular to the loading direction. The parallel probes in the two main directions of the surface derived the deformation of the test samples in both axes and calculated the displacement within the initial and deformed images. Stress-strain curves were obtained by synchronising the output of the testing machine and the DIC software. A bilinear pattern of stress-strain curve for all samples from each tree and each MC group was derived using nonlinear curve-fitting (data-fitting) using the non-linear least-squares solver of MATLAB software. By combining all four groups, the final data from each test were determined for each type of testing. The output of this step was illustrated as bilinear charts for each direction of tests. By evaluating the stress at the breakage point, the strength of linden wood in each direction for both MC groups was determined. By calculating the material properties of both HMC and LMC groups, a set of ANOVA tests was conducted to evaluate the effect of MC on the mechanical properties of the material. The MOE and MOR of both groups were calculated by Equations (4) and (5) from the bending test,

$$MOE = \frac{\left((F_{40} - F_{10})L_0^3 \right)}{4 bh^3 (\varepsilon_{40} - \varepsilon_{10})}$$
(4)

$$MOR = \frac{3F_{\text{max}}L_0}{2.hh^2}$$
 (5)

where F_{10} and F_{40} are the forces at 10 % and 40 % of the maximum force (F_{max}), and ε_{10} and ε_{40} are the deflections at these force levels. Additionally, b and h refer to the width and height of the cross-section, respectively, while L_0 denotes the span between the supports. Any correlation between MOED from NDT and MOE and MOR from static tests was analysed from the regression of their respective charts to determine the relationship between them.

2.4 Correction of material properties as an input for FEM

The FEM model was created based on Hill's theory. However, there was a notable difference between the elastic moduli for tension and compression of green wood which had to be addressed to align the material properties with the Hill's conditions (Hill 1998; Zlámal et al. 2024), according to which the MOE in tension and compression must be equal, and the tangent modulus (E_t) in directions L, R, and $T(E_{t,L}, E_{t,R}, E_{t,T})$ must be lower than the MOE.

To achieve compatibility, a trilinear model was developed for each of the three principal directions by combining two bilinear models - one for tension and one for compression. By combining the tension and compression data for each longitudinal (L), radial (R) and tangential (T) direction, a dataset of three lines was derived. The first and last lines of these datasets had a slope of 0.4 MPa, corresponding to the low tangent modulus, thereby improving the convergence of the fitting procedure (Zlámal et al. 2024). The computational model remained unchanged. The middle line, which represents the elastic region, had a slope defining an equal MOE for both compression and tension of the material. Typically, FEM models use a single MOE value for both tension and compression; however, in reality, the MOE of wood for tension and compression may differ. Dataset optimisation was based on the sum of residues from diagrams created using MATLAB software. This step resulted in three compression-tension charts for the three main directions of normal forces and three shear stress-strain charts for the three main shear directions of shear forces. These values were used as input material properties in FEM software and for subsequent analysis.

2.5 FEM modelling

Two models were prepared, one static bending test and one free vibration test. Both models were created using ANSYS Workbench software (Ansys Inc., USA) to compare the results of the FEM analysis of both tests with experimental results. The output from MATLAB was used as input for the FEM. Note that these FEM inputs were not the actual material properties but a compromise between the true properties and the constraints imposed by Hill's theory, as they did not fully satisfy the FEM convergence conditions.

The free vibration model was created using the modal analysis tool in Workbench, with mechanical physics settings. It included 69,641 eight-node hexahedral elements, each with a maximum size of 2 mm. The solver was configured for Mechanical APDL to identify 16 vibration modes.

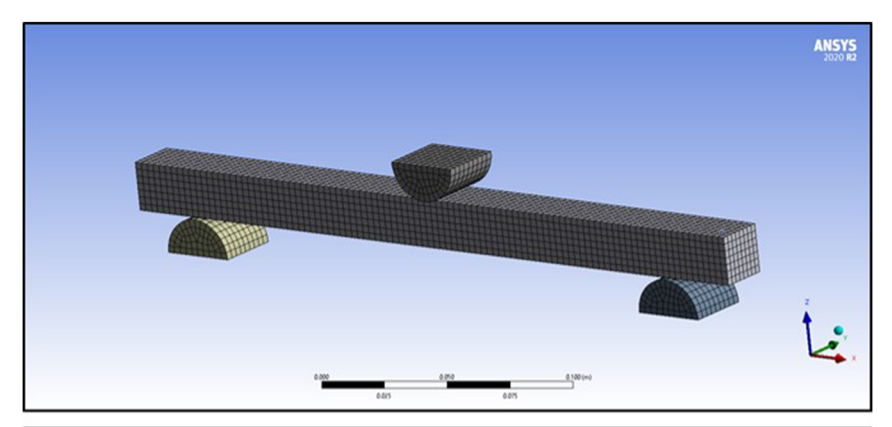
The model of the bending test was created using the static structural tool of Workbench. It had mechanical physics preferences with 6,977 eight-node hexahedron elements with a maximum size of 3 mm. A 30 sub-step analysis with program-controlled non-linear settings was chosen. The surface-to-surface contacts between the sample and the supports were modelled as sliding contacts with a friction coefficient of 0.13 based on the study of Tippner et al. (2022). Fixed supports were constrained in all directions and rotations, while the hammer was fixed except in the Z direction. The nodes at the centre of the beam were constrained along the perpendicular axis of their surface. The force-versustime curve was derived from the FEM analysis. Figure 2 presents the meshing and the boundary conditions and the displacement nodes responsible for applying the bending force in the FEM model. The symmetrical boundary conditions were applied to reduce computation costs.

2.6 Optimisation of FEM material properties

The material properties used in the FEM analysis required further refinement to make them match the experimental curves better. This optimisation was done using the targetlooking method in ANSYS Workbench (Ansys Inc., USA). The first part of the optimisation was to recognise the level of influence of each material property on the results; the next step was considering the more important parameters to be altered for optimisation. The optimization focused on aligning the FEM bending curve with the experimental data. The effectiveness of the optimisation was judged by how well the two curves matched. The experimental data were divided into 10 % intervals, which served as targets for improving the FEM model. The final optimised material properties for the linden wood were determined by refining the model using ANSYS Workbench's optimisation tool.

2.7 Statistical analysis

To evaluate the influence of MC and the orientation of growth rings on the test outcomes, the median results under the influence of different parameters were compared. Additionally, the magnitude of this influence was studied using analysis of variance (ANOVA) performed in Excel. This efficient and straightforward analysis indicated whether the results were significantly affected by the MC and orientation



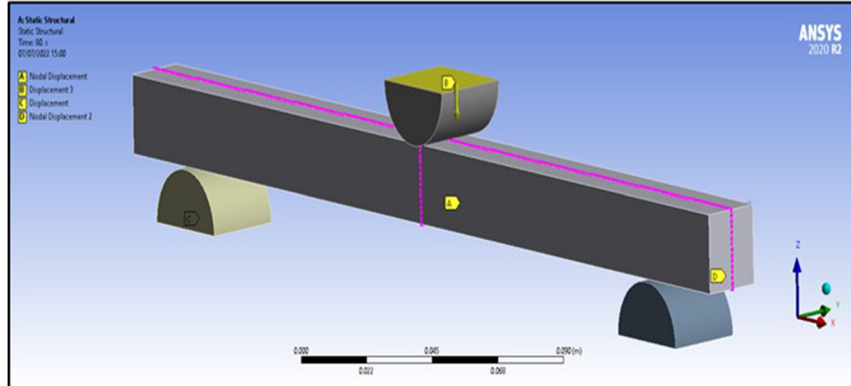


Figure 2: The schematic of the meshing and the boundary conditions of finite element model of a bending test.

of the growth rings. A P-value of 0.05 was used to accept or reject the null hypothesis.

3 Results and discussion

3.1 Vibro-acoustic testing

The dynamic properties of the linden wood were assessed using NDT on the samples before the destructive tests. Table 2 presents the median and coefficient of variation (CV) of the parameters obtained from these NDT assessments, such as frequency (FR), MOED and tangent delta ($tan\delta$).

Table 2: Dynamic properties of high moisture content (HMC) and low moisture content (LMC) linden wood (where FR is frequency, MOED is the dynamic modulus of elasticity, $tan\delta$ is tangent delta).

	HMC sa	mples	LMC sa	LMC samples		
	Median	CV (%)	Median	CV (%)		
FR _{LT} (Hz)	605	9	749	11		
FR _{LR} (Hz)	595	10	755	10		
Density (kg/m³)	970	10.6	580	13.3		
MOED _{LT} (MPa)	6,050	18.9	6,560	14.1		
MOED _{LR} (MPa)	6,260	20.0	6,610	14.4		
$ an\!\delta_{\scriptscriptstyle m LT}$	0.016	128.4	0.015	68.1		
$tan\delta_{LR}$	0.016	85.7	0.013	71.8		

The differences between median MOED_{LR} and MOED_{LT} (approximately 3% greater for the HMC group and 1% for the LMC group) were shown by the Anova test to be negligible. Likewise, the higher median MOED – about 8 % for the $MOED_{LT}$ and 6% for the $MOED_{LR}$ – in the LMC group of samples also proved to be negligible with a p-value higher than 0.05. The values for MOED were very different (more than 100 %) from those reported by Šilinskas et al. (2021) for an NDT of green wood, which is understandable as the test methods were very different.

The median of $tan \delta_{LR}$ for both the LMC and HMC groups was lower than the median of their $tan\delta_{LT}$; however, the ANOVA test showed that $an\delta_{
m LR}$ and $an\delta_{
m LT}$ were not statistically different for either the HMC or LMC group. Also, comparing the median of the $tan\delta$ for HMC and LMC indicates that the increase in MC affects the $tan\delta$; however, yet again, the ANOVA test showed that the difference between these parameters was negligible.

FR was lower in samples with higher MC by 23 % for FR_{LT} and 26 % for FR_{LR}. Figure 3 is a boxplot of MOED and $an\!\delta$ for both the LR and LT directions in the HMC and LMC groups. The LMC group exhibits a lower coefficient of variation. The differences between the NDT test values for LMC and HMC samples were expected, given the fact HMC samples had a greater range of densities than the LMC samples due to the higher water content in the HMC samples.

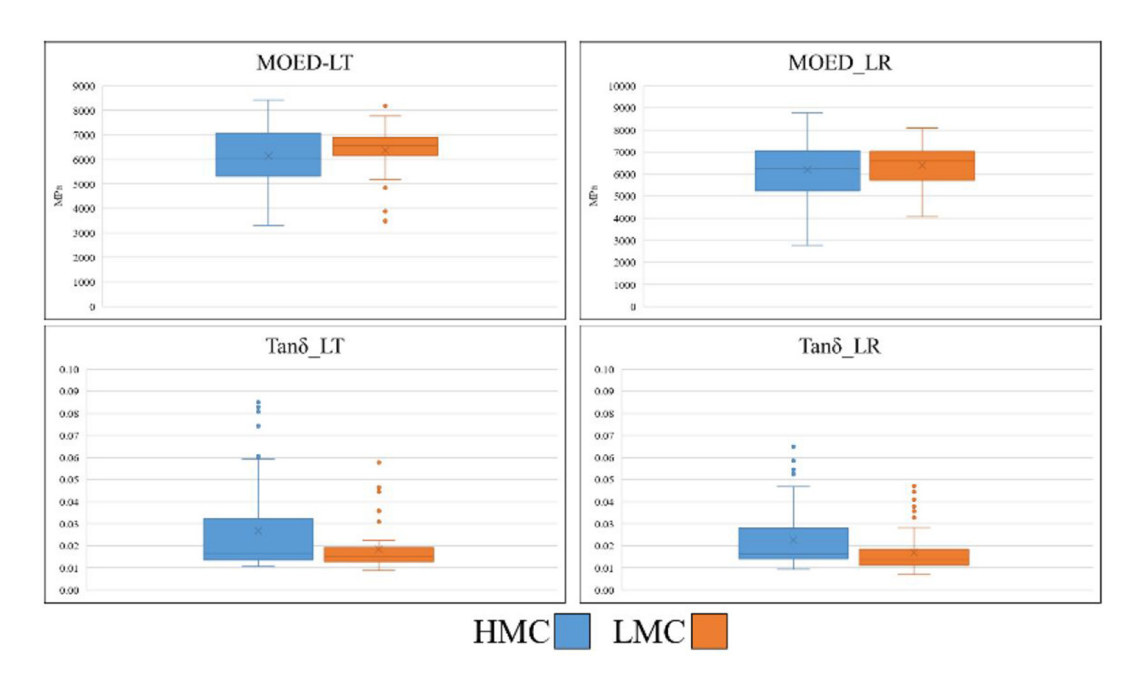


Figure 3: Dynamic modulus of elasticity (MOED) and tangent delta (tanδ) for high moisture content (HMC) and low moisture content (LMC) linden wood.

3.2 Static mechanical testing

Figures 4 and 5 display the stress-strain curves for each test on LMC and HMC samples, respectively, as well as the combined results. Each line corresponds to the test samples obtained from each tree. By aggregating the results from all test samples, a comprehensive stress-strain curve is derived. The bilinear chart, which represents the aggregated data from all samples, provides the material properties.

These material properties are derived solely from experimental data. They can be used directly in applications that do not require specific adjustments. Table 3 provides the

material properties of linden wood and reveals that the MOE in the longitudinal axis was more than four times higher than in the radial direction and 10 times higher than in the tangential direction. In the longitudinal axis, the compressive MOE exceeds the tensile MOE, whereas, in the radial and tangential directions, the compressive MOE is lower than the tensile MOE. Despite the MOE in the radial and tangential directions being much lower than in the longitudinal direction, the MOE in the radial direction was significantly higher than in the tangential direction, approximately 40 % higher for compression and around 200 % higher for tension.

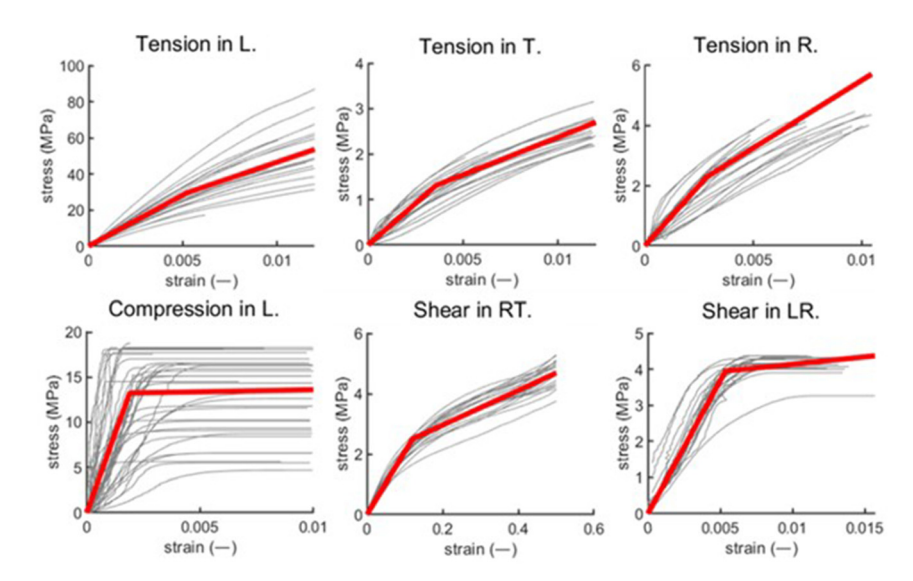


Figure 4: Stress-strain curves from tests on the low moisture content samples.

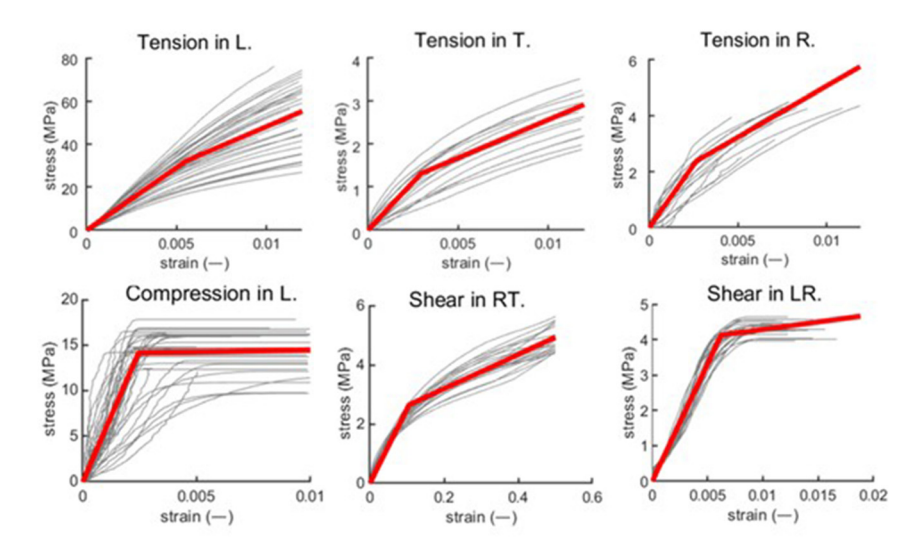


Figure 5: Stress-strain curves from tests on the high moisture content samples.

Table 3: Material properties of high moisture content (HMC) and low moisture content (LMC) linden wood (E is the normal elastic modulus, σ is yield stress, E_t is the tangent modulus, G is shear modulus, G_t is tangent shear modulus, μ Poisson's ratio, ρ density, MOE the bending modulus of elasticity, and MOR is the modulus of rupture in bending. The L, R, and T are representing longitudinal, radial and tangential directions).

	HMC s	amples	LMC samples		
	Tension	Compression	Tension	Compression	
E_L (MPa)	5,800 ± 1,300	6,270 ± 2,490	5,660 ± 1,410	7,640 ± 4,920	
E_R (MPa)	$1,070 \pm 538$	202 ± 27	768 ± 253	184 ± 45	
E_T (MPa)	435 ± 219	144 ± 19	381 ± 132	136 ± 16	
σ_L (MPa)	33.1 ± 11	14.2 ± 2	32.4 ± 12.6	13 ± 4.1	
σ_R (MPa)	2.1 ± 0.7	2.9 ± 0.0	2.1 ± 0.6	2.6 ± 0.4	
σ_T (MPa)	1.5 ± 0.2	2.2 ± 0.2	1.4 ± 0.3	2.3 ± 0.3	
$E_{t,L}$ (MPa)	$3,470 \pm 1,130$	14 ± 12	$3,430 \pm 980$	16 ± 17	
$E_{t,R}$ (MPa)	420 ± 70	3 ± 0	450 ± 120	4 ± 2	
$E_{t,T}$ (MPa)	150 ± 20	3 ± 1	150 ± 20	3 ± 1	
G_{LR} (MPa)	660 ± 80		740 ± 130		
G_{RT} (MPa)	30 ± 4		20 ± 2		
G_{LT} (MPa)	580 ± 80		680 ± 140		
σ_{LR} (MPa)	4.1 ± 0.2		3.9 ± 0.2		
σ_{RT} (MPa)	1.6 ± 0.2		1.6 ± 0.2		
σ_{LT} (MPa)	4.4 ± 0.4		4.4 ± 0.4		
$G_{t,LR}$ (MPa)	43 ± 16		41 ± 12		
$G_{t,RT}$ (MPa)	12 ± 2		11 ± 1		
$G_{t,LT}$ (MPa)	55 ± 19		55 ± 16		
μ_{LR}	0.50 ± 0.14		0.52 ± 0.25		
μ_{LT}	0.42 ± 0.23		0.47 ± 0.14		
μ_{TR}	0.49 ± 0.03		0.43 ± 0.06		
μ_{RT}	0.72 ± 0.10		0.74 ± 0.08		
$\mu_{\scriptscriptstyle RL}$	0.03 ± 0.01		0.02 ± 0.01		
μ_{TL}	0.03 ± 0.01		0.03 ± 0.02		
ρ (kg/m 3)	810 ± 35		660 ± 68		
MOE (MPa) (fit)	4,670 ± 790		4,580 ± 470		
MOR (MPa)	31.3 ± 4.7		31.4 ± 2.7		

The shear modulus in the radial-tangential (G_{RT}) direction was notably smaller (by about 5%) than in the other directions. The yield stress in the longitudinal direction was more than 16 times greater than in the other axes. Additionally, the yield stress in compression was almost identical for the radial and tangential directions, but differed significantly in the longitudinal direction. The ANOVA test results showed the p-values for all E measurements in the HMC and LMC groups were greater than 0.05, indicating no statistically significant effect of MC on these properties. Also, the ANOVA test comparing the MOE and MOR for both HMC and LMC also yielded p-values higher than 0.05, indicating no significant difference between the MOE and MOR of the HMC and LMC groups.

Table 4 presents the values for strength in different directions for the HMC and LMC groups. These values can be used as a final criterion for modelling the material, in conjunction with the maximum strains. The fibre direction significantly influences the strength of wood under both tensile and compressive loads. However, the shear strength of both groups appears to be much less affected by the fibre orientation. ANOVA tests showed negligible differences in strength values between HMC and LMC, indicating that an MC higher than FSP does not affect wood strength.

The MC samples tested in previous research varied significantly, with values of 80 % and 50 % reported by Green et al. (1999) and Niklas and Spatz (2010), respectively. A comparison of research results with those in the literature reveals notable differences. E_L differs by approximately 16 %, 19.5 % and 50 % from studies by Green et al. (1999); Niklas and Spatz (2010) and Wessolly and Erb (2017), respectively. Maximum compression parallel to the grain shows variations ranging from 4.6% compared to Green

Table 4: The ultimate stress of the high moisture content (HMC) and low moisture content (LMC) groups in different directions (u_T , u_C , and u_G , are the ultimate stress in tension, compression and shear respectively in L, R, and T directions).

	HMC san	nples	LMC samples		
	Med (MPa)	CV (%)	Med (MPa)	CV (%)	
$u_{T,L}$	55.7	24.2	50	27.4	
$u_{T,R}$	4.3	11.6	4.0	7.5	
$u_{T,T}$	2.9	10.3	2.9	6.9	
$u_{C,LR}$	14.6	13.7	15.4	22.7	
$u_{C,RT}$	3.0	6.7	2.9	10.3	
$u_{C,TR}$	2.3	8.7	2.5	8.0	
$u_{G,LR}$	4.3	4.7	4.1	4.9	
$u_{G,LT}$	4.7	6.4	4.6	19.5	
$u_{G,RT}$	4.9	8.2	4.9	6.1	

et al. (1999) to 26.7% and 44% differences compared to Niklas and Spatz (2010) and Wessolly and Erb (2017), respectively. The maximum shear values align closely with Green et al. (1999), differing by only 4.8%. However, the maximum compression perpendicular to the grain differs by more than 121% from the values reported by Green et al. (1999). It should be noted that previous researchers often considered wood as a transversely isotropic material, without distinguishing between radial and tangential directions, which may account for some of the discrepancies.

A regression analysis between MOR/MOE and MOED was conducted by fitting the charts for both LMC and HMC groups. The results revealed a strong linear relationship in the LMC group, as indicated by high coefficient of determination (R^2) values, while the HMC group showed a weak

correlation, with low R^2 values. Figure 6 presents the MOED_{LT}-MOE and MOED_{LT}-MOR charts of both groups, along with the corresponding regression analyses.

For the HMC relationships the R^2 values shows very low significance compared to LMC. The difference in R^2 values between the LMC and HMC groups may be attributed to the variation in their standard deviations, which were small for the LMC group (10 % for MOE and 9 % for MOR) and larger for the HMC group (17 % for MOE and 15 % for MOR). Similar studies have reported high regression values for MOED versus MOE, (with R^2 values of 0.8 and 0.81), and for MOED versus MOR, (with R^2 values of 0.7 and 0.43), in oak and beech samples with MC levels between 50 % and 101 % (Nop et al. 2024). These results indicate that, the R^2 values for MOED-MOR were lower than those for MOED-MOE.

3.3 FEM modelling - static bending test

According to the results presented in Table 2, there is a notable difference between the material properties of wood under different types of loading of tension and compression. However, as was mentioned in the methodology, the material properties of wood such as elastic modulus must be the same for both tension and compression to fit Hill's theory. Figures 7 and 8 provide a graphical comparison of the material properties before and after optimisation. The values shown in these updated charts were used for modelling in the FEM.

Although the material properties were optimised for use in the FEM, further refinement of the optimisation is still necessary. To validate the numerical model, the three-point bending simulation – using the optimised material

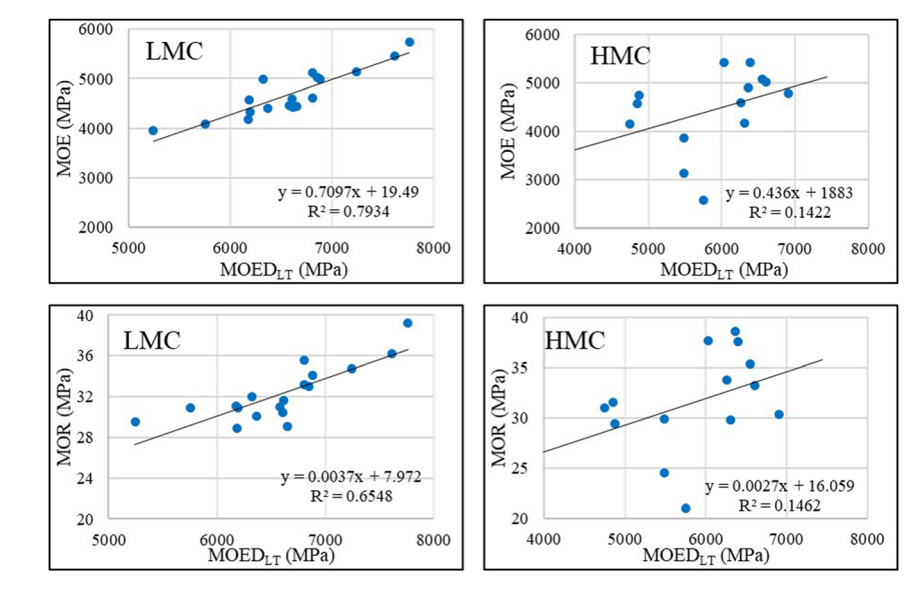


Figure 6: Linear regression between dynamic modulus of elasticity (MOED) and modulus of rupture in bending (MOR) and the bending modulus of elasticity (MOE) for the high moisture content (HMC) and low moisture content (LMC) groups.

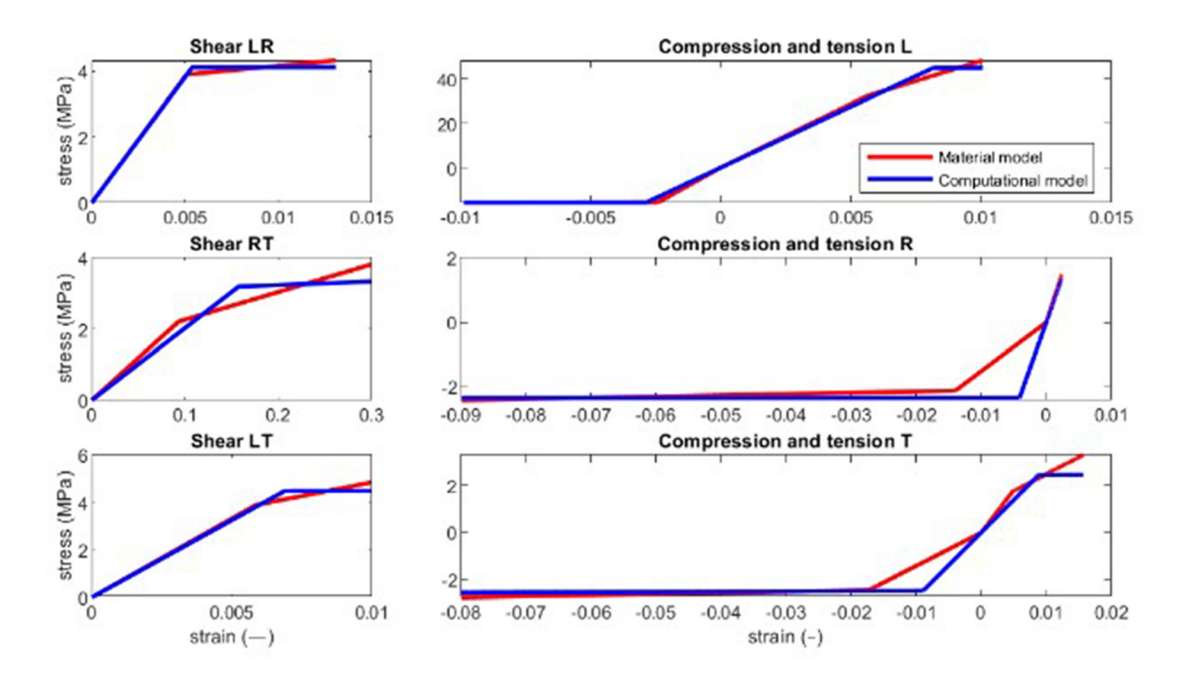


Figure 7: Modified stress-strain curves of low moisture content group.

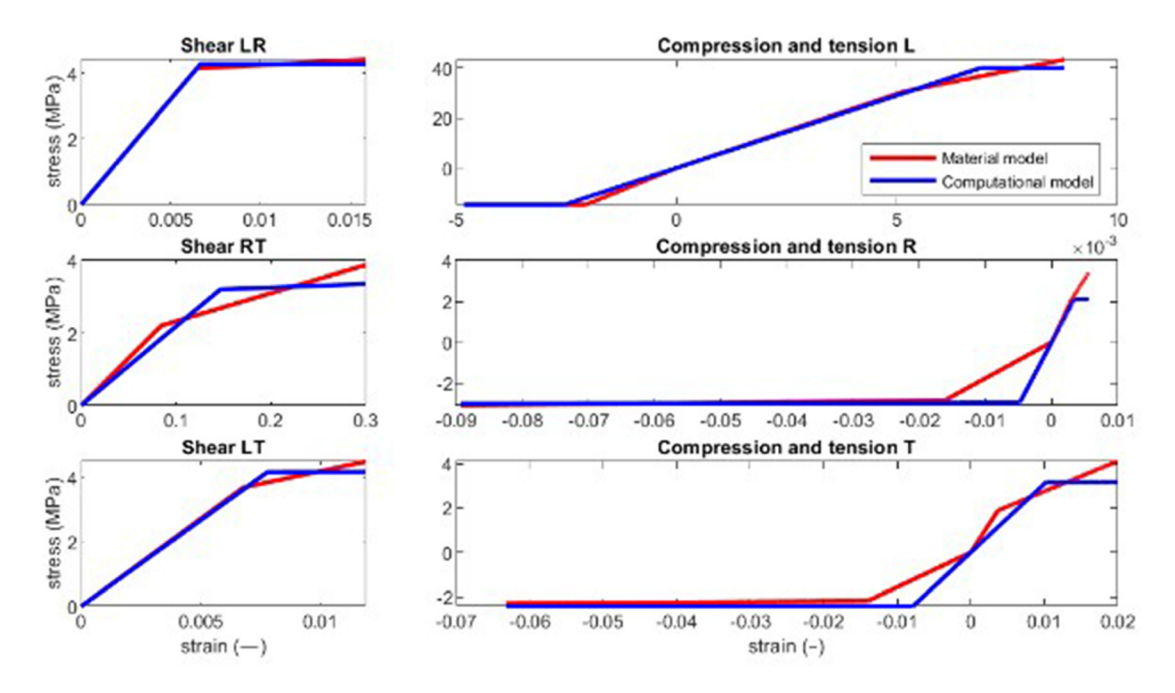


Figure 8: Modified stress-strain curves of high moisture content group.

constants – was compared with experimental data obtained from static bending tests. The optimisation tool in Workbench demonstrated the impact of certain material properties on the force-time diagram, indicating that the elastic response primarily depends on the E_L . However, as the material transitions into the plastic region, the dependency on E decreases, and other factors, such as the tensile and compressive σ_L and σ_T , become more significant. To improve accuracy, the material properties should be further optimised by focusing on the most influential parameters. After finalising the optimisation, the model's density must be defined to ensure it accurately represents natural frequencies and resonance detection for the structures. Using the Modal Analysis tool in Workbench, with frequency optimisation as the goal, the density was adjusted so that the improved material properties could be effectively applied in

Table 5: Optimised material properties of high moisture content (HMC) and low moisture content (LMC) linden wood samples (E is the normal elastic modulus, σ is yield stress, E_t is the tangent modulus, G is shear modulus, G is tangent shear modulus, G Poisson's ratio, G density. G And G are representing longitudinal, radial and tangential directions).

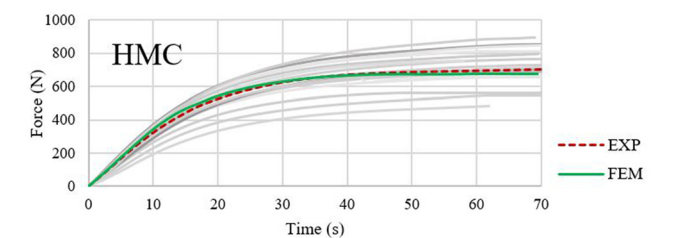
	НМС	LMC
E_L (MPa)	6,020	6,230
E_R (MPa)	880	680
E_T (MPa)	240	260
σ_{+L} (MPa)	44.0	68.2
σ_{+R} (MPa)	2.4	2.8
σ_{+T} (MPa)	2.2	2.6
σ_{-L} (MPa)	15.0	13.1
σ_{-R} (MPa)	2.3	2.9
σ_{-T} (MPa)	2.5	3.0
$E_{t,L}$ (MPa)	0.4	0.4
$E_{t,R}$ (MPa)	0.4	0.4
$E_{t,T}$ (MPa)	0.4	0.4
G_{LR} (MPa)	660	730
G_{RT} (MPa)	20	20
G_{LT} (MPa)	580	670
σ_{LR} (MPa)	4.3	4.1
σ_{RT} (MPa)	2.9	2.7
σ_{LT} (MPa)	4.6	4.6
$G_{t,LR}$ (MPa)	0.4	0.4
$G_{t,RT}$ (MPa)	0.4	0.4
$G_{t,LT}$ (MPa)	0.4	0.4
μ_{LR}	0.49	0.49
μ_{LT}	0.51	0.47
μ_{RT}	0.72	0.74
ρ (kg/m ³)	820	550

FEM modal analysis. The values of these optimised material properties are given in Table 5.

Figure 9 displays the force versus time charts for the HMC and LMC groups, respectively. The results show a strong correlation between the experimental and FEM results, with a maximum difference of 5 % which is a similar value of accuracy to the results of Zlámal et al. (2024). The grey lines represent the bending results for individual samples. The median values from the experimental data are closely aligned with the FEM results. The optimised material properties are precise and can be reliably used for modelling to achieve high accuracy in the outputs.

3.4 FEM modelling – modal analysis

The modal analysis of the beam using FEM software revealed a strong correspondence with experimental results, with maximum errors of 3.9 % for the HMC and 5.4 % for the LMC group. Table 6 presents the natural frequencies of the beam derived from the modal analysis tool in ANSYS Workbench,



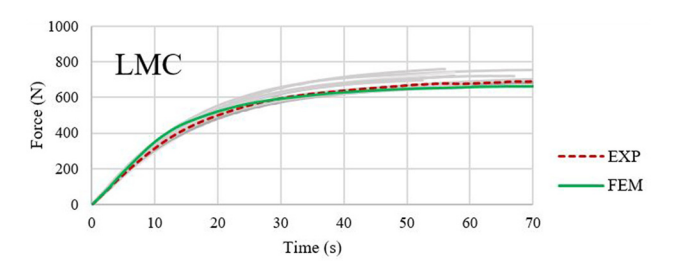


Figure 9: The force-time curve for experimental and FEM methods for high moisture content (HMC) and low moisture content (LMC) samples.

Table 6: The natural frequency of the beam in FEM software and optimised density values (FR_{LT} is the first natural frequency in longitudinal-radial bending and FR_{LR} is the first natural frequency in longitudinal-tangential bending).

		HMC samples			LMC samples		
	EXP	FEM	Diff (%)	EXP	FEM	Diff (%)	
FR _{LT} (Hz)	605	597	1.3	748	748	0.1	
FR _{LR} (Hz)	595	599	0.6	755	749	0.8	
ρ (kg/m ³)	883	820	7.2	583	545	6.4	

based on the optimised material properties. The table also includes the actual density used as input for FEM and the corresponding differences.

4 Conclusions

This article presents the material properties of linden green wood derived from experimental measurements and optimised FEM models, both static and dynamic. The experimental data may be used to enhance research by providing a basis for comparing species or MC and are suitable for use in both experimental and analytical methods. The results highlight the significant impact of MC on some mechanical properties, with differences in the elastic modulus between LMC and HMC ranging from 2 to 28 %. However, the ANOVA tests which were done for assessing the severity of the effect of MC on the mechanical properties showed that some parameters such as MOED_{LR}, MOED_{LT}, $\tan \delta_{LR}$, $\tan \delta_{LR}$, MOE and

MOR would have negligible influence from the variation of the MC levels higher than the fiber saturation point. The direction of the wood fibres greatly influences the properties; for example, the maximum strength in the longitudinal direction was over 20 times greater than in the tangential direction. Additionally, the type of loading significantly affects the material, with differences in the elastic modulus between tensile and compressive loadings ranging from 60 to 80 % in both tangential and radial directions. The modified material properties are suitable for FEM, as they have been adjusted to meet FEM conditions, unlike the unmodified parameters. These optimised properties can be used as input for FEM software to model linden green wood accurately. The results indicate that the difference between elastic moduli for tension and compression cannot be ignored; both values should be considered to determine a single MOE. However, since FEM typically requires a single value for elastic modulus, strength and tangent modulus for both tension and compression, compromises were made to align with FEM requirements while still predicting the wood's behaviour accurately. The optimized FEM models showed good agreement with experimental results, with a maximum error of 5.4 %. The NDT results provided in this article can serve as a valuable resource for those requiring a database for this type of measurement. The experimental data offer improved insights for interpreting results from device-supported tree stability assessments. Furthermore, the optimised models can enhance predictions of a tree's mechanical response under loading, contributing to more accurate evaluations of public safety and other applications.

Research ethics: Not applicable. Informed consent: Not applicable.

Author contributions: All authors have accepted responsibility for the entire content of this manuscript and approved its submission.

Use of Large Language Models, AI and Machine Learning **Tools:** During the preparation of this work the authors used Grammarly and ChatGPT by OpenAI software in order to find the primary English language grammatical mistakes in the text. After using this tool, the authors reviewed and edited the content as needed and take full responsibility for the content of the published article.

Conflict of interest: The authors state no conflict of interest. **Research funding:** This work was supported by the Ministry of Education, Youth and Sports of the Czech Republic (Grant number #LL1909, ERC CZ).

Data availability: The data used in this study are available from the corresponding author on reasonable request.

References

- Aimene, Y.E. and Nairn, I.A. (2015). Simulation of transverse wood compression using a large-deformation, hyperelastic-plastic material model. Wood Sci. Technol. 49: 21-39.
- Autengruber, M., Lukacevic, M., and Füssl, J. (2020). Finite-element-based moisture transport model for wood including free water above the fiber saturation point. Int. J. Heat Mass Tran. 161: 120228.
- Babiak, M., Gaff, M., Sikora, A., and Hysek, Š. (2018). Modulus of elasticity in three-and four-point bending of wood. Compos. Struct. 204:
- Borůvka, V., Novák, D., and Šedivka, P. (2020). Comparison and analysis of radial and tangential bending of softwood and hardwood at static and dynamic loading. Forests 11: 896.
- Brabec, M., Tippner, J., Sebera, V., Milch, J., and Rademacher, P. (2015). Standard and non-standard deformation behaviour of European beech and Norway spruce during compression. Holzforschung 69:
- Brabec, M., Lagaňa, R., Milch, J., Tippner, J., and Sebera, V. (2017). Utilization of digital image correlation in determining of both longitudinal shear moduli of wood at single torsion test. Wood Sci. Technol. 51:
- Briggert, A., Olsson, A., and Oscarsson, J. (2016). Three-dimensional modelling of knots and pith location in Norway spruce boards using tracheid-effect scanning. Europ. J. Wood Wood Prod. 74: 725-739.
- Brudi, E. and van Wassenaer, P. (2002) Trees and statics: nondestructive failure analysis. In: Tree structure and mechanics conference proceedings: how trees stand up and fall down. ISA, Champaign, IL, pp. 53-69.
- Büyüksarı, Ü., As, N., Dündar, T., and Korkmaz, O. (2017). Micro-mechanical properties of oak wood and comparison with standard-sized samples. Maderas. Cienc. y Tecnol. 19: 481-494.
- Čecháková, V., Rosmanit, M., and Fojtik, R. (2012). FEM modeling and experimental tests of timber bridge structure. Procedia Eng. 40: 79-84.
- ČSN 49 0115. (1979). Wood. Determination of the modulus of rupture in static bending [in Slovak]. Office for Standardization and Measurement,
- ČSN 49 0116. (1986). Wood. Method for determination of modulus of elasticity in static bending [in Slovak]. Office for Standardization and Measurement, Prague.
- Dahle, G.A., James, K.R., Kane, B., Grabosky, J.C., and Detter, A. (2017). A review of factors that affect the static load-bearing capacity of urban trees. Arboricu. Urban For. 43: 89-106.
- De Borst, K., Jenkel, C., Montero, C., Colmars, J., Gril, J., Kaliske, M., and Eberhardsteiner, J. (2013). Mechanical characterization of wood: an integrative approach ranging from nanoscale to structure. Comput. Struct. 127: 53-67.
- Detter, A., Van Wassenaer, P., and Rust, S. (2019). Stability recovery in London Plane trees eight years after primary anchorage failure. Arboricu. Urban For. 45: 279-288.
- Fajdiga, G., Rajh, D., Nečemer, B., Glodež, S., and Šraml, M. (2019). Experimental and numerical determination of the mechanical properties of spruce wood. Forests 10: 1140.
- Fortino, S., Mirianon, F., and Toratti, T. (2009). A 3D moisture-stress FEM analysis for time dependent problems in timber structures. Mech. Time-Dependent Mater. 13: 333-356.
- Glass, S.V. and Zelinka, S.L. (2021). Moisture relations and physical properties of wood. In: Wood handbook, wood as an engineering material. General Technical Report FPL-GTR-190. U.S. Department of

- Agriculture, Forest Service, Forest Products Laboratory, Madison, WI, pp. 4-1.
- Green, D.W., Winandy, J.E., and Kretschmann, D.E. (1999). Mechanical properties of wood. In: Wood handbook. Wood as an engineering material, Available at: https://www.fs.usda.gov/treesearch/pubs/7149.
- Guindos, P. (2014). Numerical modeling of timber with knots: the progressively damaged lattice approach vs. the equivalent damaged continuum. Holzforschung 68: 599-613.
- Guindos, P. and Guaita, M. (2013). A three-dimensional wood material model to simulate the behavior of wood with any type of knot at the macro-scale. Wood Sci. Technol. 47: 585-599.
- Guyott, C.C.H., Cawley, P., and Adams, R.D. (1986). The non-destructive testing of adhesively bonded structure: a review. J. Adhes. 20: 129-159
- Hackspiel, C., De Borst, K., and Lukacevic, M. (2014). A numerical simulation tool for wood grading model development. Wood Sci. Technol. 48:
- Hassan, K. and Tippner, J. (2019). Acoustic properties assessment of neem (Azadirachta indica A. Juss.) wood from trees irrigated with secondarily treated wastewater. BioResources 14: 2919-2930.
- Hassan, K.T., Horáček, P., and Tippner, J. (2013). Evaluation of stiffness and strength of Scots pine wood using resonance frequency and ultrasonic techniques. BioResources 8: 1634-1645.
- Hassan Vand, M. and Tippner, J. (2024). The effect of moisture content over the fibre saturation points on the impact strength of wood. Roy. Soc. Open Sci. 11: 231685.
- Hild, F. and Roux, S. (2006). Digital image correlation: from displacement measurement to identification of elastic properties – a review. Strain 42: 69-80.
- Hill, R. (1998). The mathematical theory of plasticity, Vol. 11. Oxford University Press, Oxford.
- Hu, W., Chen, B., and Zhang, T. (2021). Experimental and numerical studies on mechanical behaviors of beech wood under compressive and tensile states. Wood Res. 66: 27-38.
- Huang, C., Gong, M., Chui, Y., and Chan, F. (2020a). Mechanical behaviour of wood compressed in radial direction; part I. New method of determining the yield stress of wood on the stress-strain curve. I. Bioresour. Bioprod. 5: 186-195.
- Huang, C., Chui, Y., Gong, M., and Chana, F. (2020b). Mechanical behaviour of wood compressed in radial direction: part II. Influence of temperature and moisture content. J. Bioresour. Bioprod. 5: 266-275.
- Hum-Hartley, S. (1978). Nondestructive testing for heritage structures. Bull. Assoc. Preserv Technol. 10: 4-20.
- Ilic, J. (2001). Relationship among the dynamic and static elastic properties of air-dry Eucalyptus delegatensis R. Baker. Holz als Roh- und Werkst. 59: 169-175.
- Ilic, J. (2003). Dynamic MOE of 55 species using small wood beams. Holz als Roh- und Werkst. 61: 167-172.
- Kandler, G., Füssl, J., and Eberhardsteiner, J. (2015). Stochastic finite element approaches for wood-based products: theoretical framework and review of methods. Wood Sci. Technol. 49: 1055-1097.
- Kane, B. and Clouston, P. (2008). Tree pulling tests of large shade trees in the genus Acer. Arboric. Urban For. 34: 101.
- Korkut, S. (2011). Physical and mechanical properties and the use of lesserknown native Silver Lime (Tilia argentea Desf.) wood from Western Turkey. African J. Biotechnol. 10: 17458-17465.
- Kovryga, A., Stapel, P., and van de Kuilen, J.W.G. (2020). Mechanical properties and their interrelationships for medium-density European hardwoods, focusing on ash and beech. Wood Mater. Sci. Eng, 15: 289-302.

- Kunneman, B.P.A.M. and Albers, M.R.J. (1991) Linden trees (Tilia spp.). In: Trees III. Springer, Berlin, Heidelberg, pp. 152-163.
- Lundström, T., Heiz, U., Stoffel, M., and Stöckli, V. (2007). Fresh-wood bending: linking the mechanical and growth properties of a Norway spruce stem. Tree Physiol. 27: 1229-1241.
- Lundström, T., Jonas, T., and Volkwein, A. (2008). Analysing the mechanical performance and growth adaptation of Norway spruce using a nonlinear finite-element model and experimental data. J. Exp. Bot. 59: 2513-2528
- Mackerle, J. (2005). Finite element analyses in wood research: a bibliography. Wood Sci. Technol. 39: 579-600.
- Milch, J., Tippner, J., Sebera, V., and Brabec, M. (2016). Determination of the elasto-plastic material characteristics of Norway spruce and European beech wood by experimental and numerical analyses. Holzforschung 70: 1081-1092.
- Niemz, P. and Mannes, D. (2012). Non-destructive testing of wood and wood-based materials. J. Cult. Herit. 13: S26-S34.
- Niklas, K.J. and Spatz, H.C. (2010). Worldwide correlations of mechanical properties and green wood density. Am. J. Bot. 97: 1587-1594.
- Nop, P., Cristini, V., Zlámal, J., Vand, M.H., Šeda, V., and Tippner, J. (2024). Determination of the static bending properties of green beech and oak wood by the frequency resonance technique. Forests 15: 150.
- Pan, B. (2011). Recent progress in digital image correlation. Exp. Mech. 51: 1223-1235.
- Pan, B., Qian, K., Xie, H., and Asundi, A. (2009). Two-dimensional digital image correlation for in-plane displacement and strain measurement: a review. Meas. Sci. Technol. 20: 062001.
- Peltola, H.M. (2006). Mechanical stability of trees under static loads. Am. I. Bot. 93: 1501-1511.
- Saliklis, E.P., Urbanik, T.J., and Tokyay, B. (2003). Bilinear modelling of cellulosic orthotropic nonlinear materials. J. Pulp Pap. Sci. 29: 407–411.
- Schlotzhauer, P., Nelis, P.A., Bollmus, S., Gellerich, A., Militz, H., and Seim, W. (2017). Effect of size and geometry on strength values and MOE of selected hardwood species. Wood Mater. Sci. Eng. 12: 149-157.
- Schneeweiß, G. and Felber, S. (2013). Review on the bending strength of wood and influencing factors. A. J. Mater. Sci. 3: 41-45.
- Sebera, V., Praus, L., Tippner, J., Kunecký, J., Čepela, J., and Wimmer, R. (2014). Using optical full-field measurement based on digital image correlation to measure strain on a tree subjected to mechanical load. Trees 28: 1173-1184.
- Šilinskas, B., Povilaitienė, A., Urbaitis, G., Aleinikovas, M., and Varnagirytė-Kabašinskienė, I. (2021). The wood quality of small-leaved lime (Tilia cordata Mill.) trees in an urban area: a pilot study. Forests 12: 420.
- Smith, I., Snow, M., Asiz, A., and Vasic, S. (2007). Failure mechanisms in wood-based materials: a review of discrete, continuum, and hybrid finite-element representations. Holzforschung 61: 352-359.
- Spatz, H.C. and Pfisterer, J. (2013). Mechanical properties of green wood and their relevance for tree risk assessment. Arboricu. Urban For. 39: 218-225
- Stokes, A. (1999). Strain distribution during anchorage failure of *Pinus* pinaster Ait. at different ages and tree growth response to windinduced root movement. Plant Soil 217: 17-27.
- Sutton, M.A., Orteu, J.J., and Schreier, H. (2009). Image correlation for shape, motion and deformation measurements: basic concepts, theory and applications. Springer, New York, NY, USA.
- Tippner, J., Milch, J., Sebera, V., and Brabec, M. (2022). Elasto-plastic material model of oak at two moisture content levels. Holzforschung 76: 886-896.

Vössing, K.J. and Niederleithinger, E. (2018). Nondestructive assessment and imaging methods for internal inspection of timber. A review. Holzforschung 72: 467-476.

Wessolly, L. and Erb, M. (2017). Manual of tree statics and tree inspection. Patzer Verlag, Berlin-Hannover, Germany, p. 288.

Zink, A.G., Davidson, R.W., and Hanna, R.B. (1995). Strain measurement in wood using a digital image correlation technique. Wood Fiber Sci. 27: 346–359. Zlámal, J., Mařík, R., Vojáčková, B., Cristini, V., Brabec, M., Praus, L., and

Tippner, J. (2024). Elasto-plastic material model of green beech wood.

J. Wood Sci. 70: 1–14.